Classification of epileptiform activity in an intrahippocampal kainic acid mouse model

Vermeulen, Jeroen J.A.; Krivoshein, Georgii; Diware, Sumit; Siddiqi, Muhammad Ali; van den Maagdenberg, Arn M.J.M.; Tolner, Else A.; Hamdioui, Said; Bishnoi, Rajendra

DOI
10.1007/s42452-025-07544-7

Publication date
2025

Document Version
Final published version

Published in
Discover Applied Sciences

Discover Applied Sciences

RESEARCH Open Access

Classification of epileptiform activity in an intrahippocampal kainic acid mouse model

Jeroen J. A. Vermeulen[1†], Georgii Krivoshein[2*†], Sumit Diware[1], Muhammad Ali Siddiqi[3], Arn M. J. M. van den Maagdenberg[2,4], Else A. Tolner[2,4], Said Hamdioui[1] and Rajendra Bishnoi[1*]

[†]Jeroen J. A. Vermeulen and Georgii Krivoshein contributed equally to this work.

*Correspondence:
Rajendra Bishnoi
r.k.bishnoi@tudelft.nl
[1]Computer Engineering Lab, Delft University of Technology, Delft, The Netherlands
[2]Department of Human Genetics, Leiden University Medical Center, Leiden, The Netherlands
[3]Electrical-Engineering Department, Lahore University of Management Sciences, Lahore, Pakistan
[4]Department of Neurology, Leiden University Medical Center, Leiden, The Netherlands

Abstract

Approximately one-third of individuals with chronic epilepsy, a condition resulting from uncontrolled brain activity, do not respond to medication. Animal models are widely used to investigate the mechanism underlying epilepsy, so better drug treatments can be developed for this disease. In such studies, epileptiform activity, assessed by EEG recordings, can be used as a marker for the development of the disease. However, the analysis of EEG recordings is typically done manually, which is time-consuming, subject to observer bias, error-prone, and lacks consistency and efficiency. In this paper, we develop a novel automated methodology for detecting and classifying epileptiform activity, which is tested using the intrahippocampal kainic acid (IHKA) mouse model, a representation of human temporal lobe epilepsy. For that, EEG/LFP recordings are obtained from biological experiments using the IHKA mouse model for data acquisition. We use a spike detection method that combines an improved version of the nonlinear energy operator (NEO) with the automatic NEO thresholding (ANT) algorithm. The proposed method is implemented in Python as an automated and time-efficient algorithm, given its adaptability to different spike and epileptiform event criteria, making it suitable for use in preclinical and potentially future clinical studies. Using our proposed methodology, we achieve a 93.1% accuracy in detecting epileptiform events and a 95.8% accuracy in classification. Moreover, the time for analysis of EEG recordings was reduced by 98.8% compared to manual analysis. Additionally, to demonstrate the potential of the algorithm for brain–machine interfaces (BMI) applications, we develop a hardware architecture and implement it using both an application-specific integrated circuit (ASIC) and a field programmable gate array (FPGA). The FPGA shows the feasibility of near real-time implementation, and for our ASIC implementation, we achieve a post-layout area of 9114 μm^2 with a dynamic power consumption of 16.09 µW using TSMC 40 nm technology.

Keywords Epilepsy, Classification, Spike detection, Seizure detection, IHKA mouse model, ASIC, FPGA

1 Introduction

Epilepsy is a neurological disorder characterized by recurrent seizures, caused by abnormal and excessive neuronal activity in the brain that affects approximately 65 million people worldwide [12]. The consequences of epilepsy can be severe to patients as seizures may lead to symptoms like loss of consciousness. Prolonged inability to control these attacks can cause cognitive decline and in rare cases, may even result in the death of the patient [9]. Approximately 60% of patients with epilepsy suffer from partial (or focal) epilepsy, meaning that seizures originate in a specific region of the brain. The most common type of partial epilepsy is *Temporal Lobe Epilepsy* (TLE), which typically originates from the hippocampus, entorhinal cortex, or amygdala [10]. Around one-third of patients with TLE are resistant to medication, making it one of the most drug-resistant types of epilepsy [7]. Preclinical studies in rodents in which epilepsy is evoked are performed to investigate the underlying disease mechanisms in search of new treatments for epilepsy. A commonly used model for studying TLE and effects of anti-seizure drugs is the intrahippocampal Kainic Acid (IHKA) mouse model. In this model, a status epilepticus is induced by unilateral hippocampal kainate injection, that initiates the development of chronic epilepsy consisting in recurrent focal hippocampal epileptiform activity [3, 5, 23, 25] epileptiform activity, i.e. excessive, uncontrolled and highly synchronized neuronal network activity [21], is visible in electroencephalography (EEG) or local field potential (LFP) recordings and traditionally analyzed manually by experts. As preclinical studies typically generate a lot of longitudinal EEG/LFP recordings, visual analysis is a time-consuming process and prone to observer bias and error [2]. The epileptiform activity detected in EEG/LFP recordings can be categorized into two main types: isolated spikes and epileptiform events. The epileptiform events can be classified into various subgroups based on, e.g. their duration or frequency features of the network activities within the event [23]. All forms of epileptiform activity can potentially serve as indicators of the progression of epilepsy.

Several commercial software packages are available that offer spike and/or burst detection features [14, 15], while open-source efforts have produced tools to detect epileptiform activity, extract spikes, and classify events into different subgroups [8, 22, 24, 27]. In general, spikes can be detected using automatic spike detectors for which multiple methods exist, such as thresholding, energy operators, and machine learning models [6, 17, 28], whereas the epileptiform event classification is typically model-specific given variation in epileptiform event features across epilepsy models. Implementing a robust and automated analysis method is essential for any epilepsy model, as spike morphologies can vary widely, and noise levels often fluctuate across time and datasets.

A few efforts to automate the detection of epileptiform events using data from different animal epilepsy models have been made already. For instance, Kyle et al. [8] developed a method to extract both spikes and epileptiform events by first applying spike detection using amplitude thresholding and subsequently detection of epileptiform events. Although this approach is time-efficient, as it reduces manual activity, its reliance on manually set thresholds for spike detection limits its robustness to noise. Moreover, overly lenient criteria for defining epileptiform events can increase the risk of false positives. Zeidler et al. [27] introduced a method that first filters the signal and then highlights segments likely to include a behavioral seizure manifestation. While this approach reduces the time required for data analysis, it still relies on a manually set spike

threshold, which may not work consistently across different datasets. Wei et al. [24] described a machine learning based method which is more robust as it can extrapolate patterns beyond the training set. In this method, an XGBoost algorithm is introduced, trained on multiple mouse models of epilepsy and tested on a distinct epilepsy mouse model that successfully detected epileptiform events. However, this particular machine learning model is not suitable for the present study with the IHKA model, as it is trained and developed for data obtained from scalp-based EEG recordings rather than intracerebral LFP recordings. Unlike LFP, which captures localized neural network activity, EEG encompasses neural activity from the entire brain. Also, training an already implemented machine learning model, such as the XGBoost algorithm, is quite complex, as it requires an extensive labeled dataset, which in turn demands significant manual analysis. Regarding the final step of analysis, the classification of different types of epileptiform events, there is, to our knowledge, only one study, by [22], that implemented an automated analysis approach on LFP data from the IHKA model. The method used is based on a spike and event detection approach that was introduced for an encephalitis-induced epilepsy model by [1], which marks spikes based on amplitude, width, instantaneous energy, and slope. The event detection was modified by [22] to be applicable to the epileptiform activity features of the IHKA model, using the description of epileptiform event features by [23]. While that method is able to detect and classify epileptiform activity in the IHKA model, it has two clear downsides: (1) spike detection makes use of thresholds that need to be set manually, and (2) both automated spike and event detection rely on a visual analysis step, which thereby still requires time-demanding manual inspection. Developing an automated, time-efficient method that can detect and classify epileptiform activity from EEG/LFP recordings from the IHKA model would facilitate research, improve accuracy, and accelerate advancements in epilepsy altogether.

In this paper, we present a new methodology for the automated detection and classification of epileptiform activity in EEG/LFP recordings that consists of three steps and is developed using LFP data from the preclinical IHKA mouse model of epilepsy. In the first step, a spike detector is introduced using an improved version of the nonlinear energy operator (NEO) and automatic NEO thresholding (ANT) combination. Secondly, an epileptiform event detector is proposed that can detect epileptiform events using a generalized description. Finally, an epileptiform event classifier is proposed that classifies epileptiform events into one of four types using event duration and local spike frequency. The overview of the proposed real-time classification framework for epileptiform activity is illustrated in Fig. 1. The source code of the automated analysis approach is available on (https://github.com/Rajendra154/LUMC-TUD-Real-time-classification-IHKA-MM).

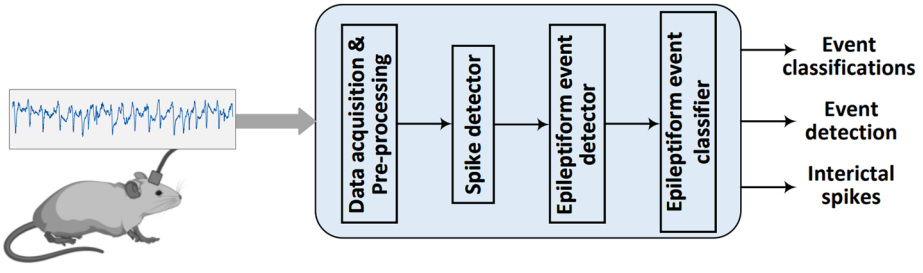

Fig. 1 Overview of the proposed real-time classification framework for epileptiform activity in the intrahippocampal kainic acid mouse model

The key contributions of this paper are:

- EEG/LFP data is acquired through real experiments conducted on the IHKA mouse model.
- We propose a new and automated method for detecting and classifying epileptiform activity in the IHKA mouse Model. The proposed method is implemented as a Python algorithm, streamlining the analysis of LFP recordings and reducing the time required for processing.
- We implement the proposed method in real-time as both an ASIC and FPGA to show the working as a Brain-Machine Interface.

The algorithm was manually verified by two animal epilepsy experts (G.K. and E.A.T.) using 108 h of hippocampal EEG/LFP recordings from the IHKA model and the results of the automated epileptiform event analysis approach show accurate detection and classification with drastically reduced analysis time compared to the manual analysis method.

The remainder of the paper is organized as follows: in Sect. 2, the IHKA mouse model is explained by going over the mice and their surgery procedure in the preclinical studies, after which descriptions of the epileptiform activity are given. Section 3 introduces the proposed epileptiform activity detector and its algorithmic implementation in Python. Section 4 introduces the proposed hardware implementation, which is implemented using VHDL and Verilog. Section 5 gives an overview of the experimental setup, and Sect. 6 goes over the results obtained; the conclusions are given in Sect. 7.

2 Intrahippocampal kainic acid model

2.1 Animals

Electrographic EEG/LFP recordings were obtained from the intrahippocampal kainic acid (IHKA) mouse model and used for the development and testing of epileptiform activity detection and classification. For the IHKA model, C57BL/6J male mice (Janvier, France) at the age of 10–12 weeks were utilized. During experimental procedures, all mice were kept under standard housing conditions (temperature of 22 ± 1.5 °C, 12/12 h light/dark cycle) with food and water *ad libitum*.

2.2 Surgery

Animals were anaesthetized with isoflurane (induction 4%; maintenance 1.5%) in pressurized air. Carprofen (5 mg/kg) was injected subcutaneously 15 min before surgery as preemptive analgesia. During surgery mice were placed in a stereotactic device. After scalp skin resection, small craniotomies were drilled in the skull using a dentist s bore (Fine Science Tools, USA). Kainic Acid (KA; 200 ng in 50 nL 0.9% NaCl; Sigma-Aldrich, USA) was injected into the CA1 region of the dorsal hippocampus (anterioposterior: − 2.0 mm; mediolateral: 1.5 mm; dorsoventral: − 1.3 mm; Fig. 2A) using a glass 0.5 µL NanoVolume on-column syringe (0.23 mm OD needle; Trajan Scientific and Medical, USA) at a rate of 0.1 µL/min controlled by a UMP2 micro-infusion pump (World Precision Instruments, USA). To limit backflow of fluid, the needle was maintained in situ for 2 min before and 5 min after injection. After surgery, mice were placed in a recovery box with temperature controlled at 30 °C for 30 min. Status epilepticus, which occurs in the hours after intrahippocampal KA injection, was monitored using video

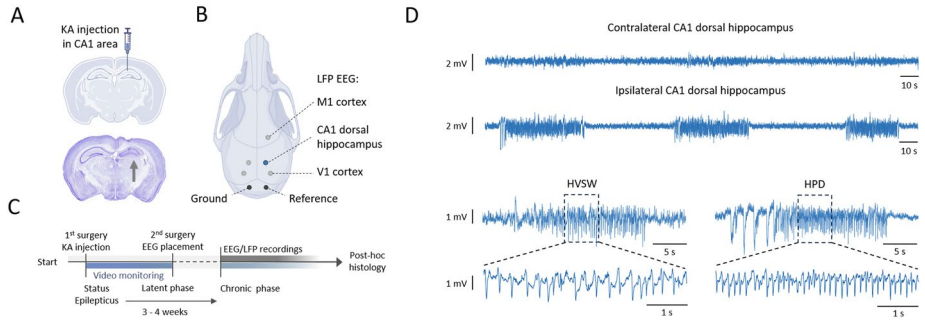

Fig. 2 EEG/LFP recordings in the IHKA mouse model. **a** Schematic of the kainic acid (KA) injection site in the CA1 area of the dorsal hippocampus assessed by post hoc histology in coronal sections. The arrow indicates the malformed (including dispersion of the normally compact cell layers) and damaged (i.e. gliosis, cell loss) ipsilateral hippocampus, indicating successful KA injection and development of an epileptogenic zone. **b** Schematic of the position of the LFP recording electrodes, whereby the LFP electrode in the right dorsal hippocampus at the site of KA injection (i.e. ipsilateral) is used for detecting the epileptiform activity in this area. **c** Experimental design of surgeries and video-EEG/LFP recordings. Of note, EEG/LFP recordings started at 5 weeks post-KA injection/status epilepticus. **d** Representative examples of LFP recordings from the contralateral and ipsilateral (site of KA injection and the epileptic focus) CA1 area of the hippocampus. The ipsilateral side contains spontaneous focal epileptiform events with hallmark electrographic characteristics typical for the IHKA model, i.e. high voltage sharp waves (HVSW) and hippocampal paroxysmal discharges (HPD). This feature of unilateral hippocampal HVSW and HPD epileptiform activity was observed in all IHKA mice used in the study

recording combined with post hoc behavioural analysis. The severity of status epilepticus was assessed using the Racine scale [19], with a modification to include an additional stage 6 defined as clonic seizures accompanied by repetitive vigorous jumping and falling around the cage. Only mice that experienced vigorous convulsive status epilepticus, defined as a status lasting longer than 3 h with recurrent seizures progressing to stages 3 6 were selected for microelectrode placement a week later. Mice were video monitored until normal behavior (defined as exploration and/or grooming) resumed and returned to their home cages.

One week later, during a second surgery, custom-made microelectrodes (75 µm platinum/iridium; PT6718, Advent Research Materials, UK) were placed in the same CA1 area and coordinates of the dorsal hippocampus (Fig. 2B). Additional micro-electrodes were placed in the contralateral hippocampus and the bilateral cortex (bilateral visual cortex V1 and motor cortex M1 ipsilateral to the hemisphere in which kainic acid was injected) to assess any spread of electrographic epileptiform activity. Reference and ground electrodes were placed in the cerebellum. Then, the micro-electrodes were connected to a 7-channel pedestal (Plastic One, USA) and secured to the skull with dental cement (DiaDent Europe, NL). All IHKA mice were confirmed by Nissl staining to display unilateral neuronal loss and gliosis in dorsal CA1-3 hippocampal regions, and dentate gyrus granule cell dispersion, in accordance with classical neuropathological features of TLE [3, 11].

2.3 EEG/LFP recordings and pre-processing

Mice were connected to the seven-channel commutator in a Faraday-shielded recording cage at week 5 post-KA injection (i.e. 5 weeks after status epilepticus) for continuous EEG/LFP and video recording during the chronic epileptic stage. The obtained LFP recordings from cortical and hippocampal regions were pre-amplified (3×), filtered (0.05 500 Hz) and amplified (200×) using custom built hardware, and digitized at 5 kHz. The data were then post-hoc down-sampled to 1 kHz for further analysis. Note that datasets

with other sampling rates can be analysed as well by adapting the sampling rate features in the source code (see line 18 to 36 in https://github.com/Rajendra154/LUMC-TUD-Real-time-classification-IHKA-MM/pulls) of the automated script analysis. After man ual inspection of 6 h of recordings/mouse in week 5 and 6 - to confirm that mice had entered the chronic epilepsy stage with frequent occurrence of HVSW and HPD events - 12 h of continuous LFP recordings were used per animal (in total 9 IHKA mice) for post-hoc analysis of epileptiform activity. Following the experiments, mice were sacrificed for histology procedures to confirm electrode locations and assess cellular damage in the KA-injected hippocampus (Fig. 2C).

2.4 Electrographic epileptiform activity

With respect to the types of epileptiform activity in the IHKA mouse model, both spikes and epileptiform events were recorded and specifically present in the ipsilateral CA1 recording. Spikes are visible in the hippocampal LFP recordings and are defined as transiently increased neuronal activity that is distinguishable from background activity with negative and positive peaks of activity. The duration of a spike was defined to range from 40 to 100 ms, and spike amplitude was defined to be larger than 1.5× the baseline amplitude of the signal. The baseline amplitude was considered to be the average amplitude of a 20-second signal segment with no epileptiform activity. Of note, the shape of a spike can vary depending on the neuron that fires, the type of epilepsy, and the stage of epilepsy. Further, spikes can be categorized as ictal or interictal, where ictal spikes are found inside epileptiform events, and interictal spikes are found outside such events.

An epileptiform event can be described as a group of spikes that follows a set of requirements with respect to spike frequency, spike amplitude, and the duration of the event. The first type of epileptiform event that occurs in the IHKA model is a spike train, which has a duration between 2 and 5 s. Within a spike train, spikes were defined to have an amplitude of at least 3× the baseline amplitude, spike frequency should be at least 2 Hz, and the interval between subsequent events should be minimally 3 s. High voltage sharp waves (HVSW) are a second form of epileptiform event in the IHKA model, with the same criteria with regard to spike frequency and amplitude and interevent interval as a spike train, i.e. spike frequency >2 Hz, spike amplitudes >3× baseline amplitude and interevent interval >3 s. HVSW duration, however, is longer than that of a spike train, ranging from 5 to 20 s. HVSW can show evolution in their spike frequency and pattern but are typically regular in terms of spiking activity. An example of HVSW is shown in Fig. 2D, in which the HVSW shows no clear evolution over time (monomorphic). The last type of epileptiform event in the IHKA model concerns hippocampal paroxysmal discharges (HPDs), which typically start with HVSW-like activity followed by spikes with an amplitude of at least 2× the baseline amplitude and a spike frequency of at least 5 Hz. Figure 2D illustrates an example of an HPD event, showing the start of the event consisting of HVSW-like activity, followed by spikes with higher frequency and lower amplitude. The figure clearly shows that HPD are polymorphic as they exhibit evolution in spike pattern and frequency. HPD events are further categorized into short HPDs (sHPDs) and ictal HPDs (iHPDs). HPD events with a duration of 5 to 10 s are classified as sHPDs and HPD events with a duration of at least 10 s are classified as iHPDs. Moreover, an HVSW event which exceeds 20 s is classified as an iHPD.

Note that in the investigated data set no generalized (convulsive) epileptiform seizures [11] were observed. Table 1 summarizes all types of recorded events together with their characteristics.

3 Proposed detector and classifier of epileptiform activity

Figure 1 presents an overview of the data flow in the proposed methodology for detecting and classifying epileptiform activity in the IHKA model, including its algorithmic implementation. The process begins with data collection and is followed by pre-processing. The source code of the final analysis approach is available on https://github.com/Rajendra154/LUMC-TUD-Real-time-classification-IHKA-MM/pulls. The pre-proc essed EEG/LFP recordings are then used as input to the spike detector, which has the detected spikes as output. These detected spikes are then processed by the epileptiform event detector to identify all types of epileptiform events. This includes distinguishing between ictal events (a subset of epileptiform events) and interictal spikes based on a general description. Finally, the event classifier categorizes events based on the above-indicated event classifications and provides outputs of the detected events, classification of the detected event and the interictal spikes.

3.1 Spike detector

Spike detection is an important part of the proposed detection and classification method, as the epileptiform event detector (and subsequent classifier) relies on the detected spikes. It is important that the spike detection method is computationally simple as it should be implemented in the hardware, must be robust to EEG/LFP noise and needs to be automated so no manual intervention is needed. The section below highlights various existing spike detection methods with their advantages and disadvantages that provide the background for the approach implemented in our spike detector. We performed a qualitative comparison of four prior methods suitable for IHKA mouse model signal processing, considering factors algorithmic complexity, speed, robustness to noise and automation.

3.1.1 Existing methods

The most basic spike detection methods make use of amplitude thresholding (AT) [6, 20], which has a low computational burden but lacks robustness with respect to noise and the change of signal characteristics in different datasets as shown in Table 2. Moreover, every dataset requires its own thresholding, which is a non-automated implementation that needs extensive manual intervention. Another commonly used method is the discrete wavelet transform (DWT) [16], which decomposes an EEG/LFP signal into different frequency components and has the advantage that it can accurately identify the timing and frequency characteristics of spikes with good noise suppression capabilities.

Table 1 Characteristics of different types of epileptiform events in the IHKA model

	Spike train	HVSW	sHPD	iHPD
Spike amplitude (× Baseline amplitude)	≥ 2	≥ 3	≥ 2	≥ 2
Spike frequency	≥ 2 Hz	≥ 2 Hz	≥ 5 Hz	≥ 5 Hz
Minimum event duration	2 s	5 s	5 s	10 s
Maximum event duration	5 s	20 s	10 s	-
Interevent interval	≥ 3 s	≥ 3 s	≥ 3 s	≥ 3 s

Table 2 Overview of spike detection methods and their advantages and disadvantages

Spike detection method	Complexity	Speed	Robustness to noise	Automatic
AT [6]	+	+	–	–
CNN [17]	–	+	+	+
DWT [16]	–	–	+	–
NEO [13] and ANT [26]	+	+	+	+

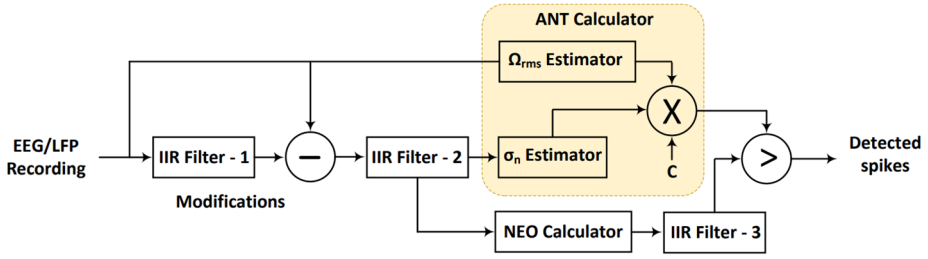

Fig. 3 Block diagram of the proposed spike detector, consisting of three IIR filters, an NEO calculator and an ANT calculator

Drawbacks of this method are that choosing an appropriate wavelet is crucial, and the method is computationally intensive. Machine learning methods are also available, such as the convolutional neural network (CNN) developed by [17]. The EEG/LFP signal is split up into different frequency bands, which helps achieve high sensitivity and accuracy. The downside is that implementing the method is computationally intensive and needs a training dataset. Lastly, energy operators, such as the amplitude slope operator (ASO) [28] and the nonlinear energy operator (NEO) [13], are methods that use instantaneous energy in a signal to detect spikes. NEO and ASO are both spike detection methods that are robust to noise and computationally efficient. NEO, in combination with automatic NEO thresholding (ANT) [26], even allows for automated spike detection using a dynamically calculated threshold.

3.1.2 Spike detector overview

A block diagram of the proposed spike detector using NEO and ANT is shown in Fig. 3. It highlights the individual components of the detector, which include the NEO calculator, three Infinite Impulse Response (IIR) filters and the ANT calculator. The ANT calculator comprises two key estimators: the root mean square (RMS) frequency (Ω_{RMS}) estimator and the standard deviation of the background noise (σ_n) estimator.

3.1.3 Nonlinear energy operator

The NEO calculator implements Equation 1, which calculates the instantaneous energy from an amplitude component, $x^2(n)$, and a frequency component, $x(n+1)x(n-1)$.

$$\psi[x(n)] = x^2(n) - x(n+1)x(n-1) \tag{1}$$

3.1.4 Infinite impulse response filters

Three IIR filters are implemented using Eq. 2, where α is the feedback coefficient and $\alpha < 1$. As shown in Fig. 3, IIR Filter 1, combined with the subtraction mechanism, represents an improvement over the circuit previously proposed [26].

This IIR filter is designed to calculate the spike amplitude while effectively eliminating temporal signal drift. The remaining two IIR filters are employed to smoothen the signal in order to improve the processing accuracy. IIR filter 1 is implemented using $\alpha = \frac{1}{300}$, filter 2 using $\alpha = \frac{1}{4}$, and filter 3 uses $\alpha = \frac{3}{32}$.

$$y(n) = \alpha x(n-1) + (1-\alpha)y(n-1) \tag{2}$$

3.1.5 Automatic NEO thresholding

ANT is implemented using Eq. 3, where C is a scalar, σ_n is the standard deviation of the noise, and Ω_{RMS} is the RMS frequency. The standard deviation of the noise and the RMS frequency are both estimated, as calculating them requires too much computational power. For the scalar, a standard value of $C = 14$ is chosen.

$$Th_{\psi} = C\sigma_n^2\Omega_{rms}^2 \tag{3}$$

Equation 4 shows the estimation of σ_n, which is obtained from the median absolute deviation (MAD) [18], where the median is taken over a window of the absolute value of the output of IIR filter 2.

$$\sigma_n^{MAD} = \frac{median(|x(n)|)}{0.6745} \tag{4}$$

The estimation of the RMS frequency is done by making use of the zero-cross frequency. Equation 5 shows the estimation, where n_z is the number of zero-crossings inside the window of size N_z. Following [26], the input signal should be the output of IIR filter 2, but the temporal drift removal also removes a lot of zero-crossings. Because of this, the signal checked for zero-crossings is the input of the spike detector.

$$\Omega_{rms} = \frac{n_z}{2N_z}\pi \tag{5}$$

The spike detector explained above does not meet the requirement for accuracy (see Sect. 6.2). To improve the accuracy, the value of C in Equation 3 can be adjusted during analysis. With the ability to adjust C and to keep the analysis time efficient, the window for both the estimation of σ_n and Ω_{RMS} is chosen to be the entire dataset as this results in just one threshold for the whole dataset.

3.2 Epileptiform event detection

The second step, as illustrated in Fig. 1, is the detection of epileptiform events. A general description of epileptiform events is made (see Table 3) to detect in this stage all types of epileptiform events. The detection method checks the signal, using the detected spikes, for events fulfilling the general description of an epileptiform event. The data requirement for the spike detection methodology includes sufficiently long and high-resolution recordings with clear amplitude variations and temporal precision to capture events of varying durations and frequencies for reliable detection and classification. To generate the algorithm, a baseline amplitude calculation is first performed to determine the

Table 3 Description of a general epileptiform event used by the event detector

Spike amplitude	Spike frequency	Event duration	Inter-event interval
$\geq 2\times$ Baseline	≥ 2 Hz	≥ 2 s	≥ 3 s

amplitude requirement. This is followed by the creation of a detection loop, and finally, a function called preliminary spikes check is implemented.

3.2.1 Baseline amplitude calculation

The first requirement defines that the spike amplitude, needs to be larger than two times the baseline amplitude, whereby the baseline amplitude is the amplitude of the signal without detected spikes. To calculate the amplitude, a signal segment of 30 s that does not contain spikes is selected, and the middle 20 s should have a noise level that is not influenced by nearby spikes. From these 20 s, the baseline amplitude is calculated by taking the 97th percentile of all samples. The baseline amplitude can change over time, and thus, the baseline amplitude is adjusted when feasible. That is, an adjustment is performed every time a segment of 30 s with no spikes is found, and the update takes place using an IIR filter with $\alpha = 0.2$.

3.2.2 Detection loop

A detection loop is incorporated to identify epileptiform events based on the general characteristics as specified in Table 3. A flowchart illustrating this detection process is provided in Fig. 4. Moreover, hardware implementation details related to this loop are

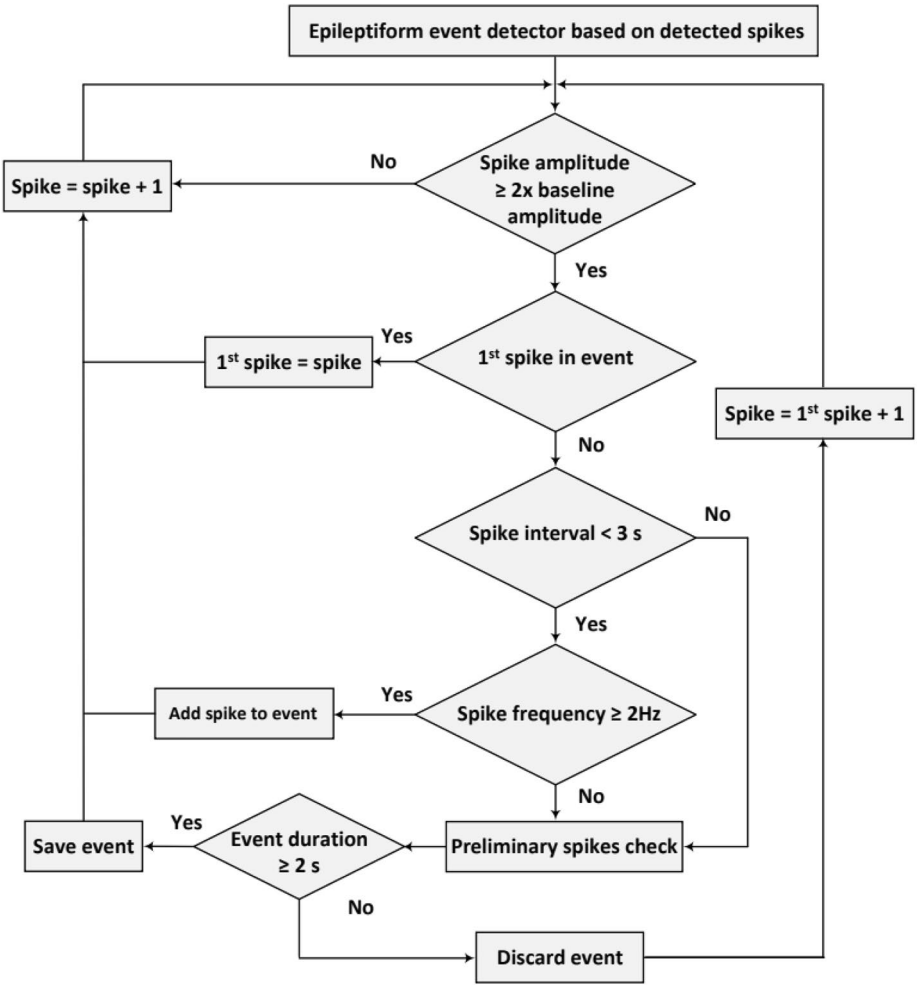

Fig. 4 Flowchart of the generalized epileptiform event detection methodology used in our implementation

discussed in Sect. 4. The algorithm systematically iterates over each detected spike to evaluate key parameters, specifically, spike amplitude, frequency, and inter-spike interval. The inter-spike interval, in this context, serves as a criterion for segmenting distinct events by ensuring that a minimum temporal separation of 3 s is maintained between successive events. Please note that the detection mechanism uses a sliding window approach to analyze spike sequences. Each new spike is added to the candidate event window and the most recent spikes are checked against predefined conditions to determine whether they conform to the characteristics of an epileptiform event. If one of the last two spikes fails to satisfy these conditions, either in terms of amplitude threshold, spike rate, or timing that the algorithm concludes the current candidate event. This step is referred to as the completion of the preliminary spike check, which is described in detail in the subsequent section. Once a preliminary candidate event is identified, its total duration is evaluated. If the duration falls below the minimum required threshold, the candidate is discarded, as it does not meet the temporal definition of a valid epileptiform event. In such a case, to avoid missing overlapping or closely spaced potential events, the detection loop resumes from the second spike of the discarded sequence (i.e., "spike = first spike + 1"). This ensures an analysis of all possible spike combinations and minimizes the risk of missing true events due to rigid windowing or segmentation. By combining parameter-based filtering with a systematic iteration strategy, this detection loop enables identification of epileptiform activity while maintaining compatibility with both algorithmic and hardware-level implementations.

3.2.3 Preliminary spikes check

As explained in Sect. 2.4, HPD events typically starts with HVSW-like activity, which results in the start of HPD events containing higher amplitude but lower frequency spikes than the rest of the event. These lower frequency spikes can reach frequencies below 2 Hz, which causes the detection loop to ignore them. However, if these spikes are within 3 s of each other and this group is within 3 s of an event, these spikes should be included with the rest of the event if a frequency of at least 2 Hz is reached. To include these, the event detection loop of Fig. 4 is run after event detection over the spikes in front of the event.

3.3 Epileptiform event classification

The classification of epileptiform events follows when the general epileptiform event detection itself is finished and is based both on the duration of an event and the spike frequency inside events. Epileptiform events were detected using the general description of Table 3. When comparing this to the content in Table 1, it is clear that the general event description closely resembles that of spike trains and HVSW events. Because of this, all events are automatically classified as spike train (if they have a duration between 2 and 5 s), as HVSW (if they have a duration between 5 to 20 s), or as iHPD (when they last longer than 20, see also description of HPD classes). Events are classified as HPD if a peak spike frequency of at least 5 Hz is reached, which is based on the description by [23], stating that an HPD event is required to have 5 continuous seconds with at least 25 spikes inside. The event detector keeps track of the peak spike frequency of 5 continuous seconds in an event and is classified as HPD if it reaches the threshold of 25 spikes/5 s, i.e. 5 Hz. The distinction between sHPD and iHPD is then made on duration.

Events between 5 and 10 s are classified as sHPD, and longer events are classified as iHPD. Note that these variables in the algorithm are parameterized to allow easy extension for broader use. This means the algorithm can be adapted to fit other event criteria, also allowing application to other preclinical epilepsy models. In the source code (available on https://github.com/Rajendra154/LUMC-TUD-Real-time-classification-IHKA-MM/pulls), details concerning the epileptiform event parameters are described in lines 18 to 36, and can be adapted, also allowing application to additional preclinical epilepsy models.

4 Hardware implementation

Hardware implementation of the epileptiform activity detector and classifier follows the structure explained in the previous section but has some adjustments to support real-time detection and classification. Future real-time implementation is possible by the immediate execution of the spike detection algorithm on hardware platforms (FPGA/ASIC) during live EEG/LFP data acquisition. The lightweight and efficient design ensures minimal processing delay, supporting operation during real-time recordings in mice. A block diagram of the system is shown in Fig. 5, which shows the interconnection of the sub-systems. The input of the system is a 16-bit signal using a two s complement and fixed-point representation. The first bit is used as a sign bit, the following four bits are used for the integer, and the last eleven bits are used for the fraction. With this representation, all values between – 16.0000 and 15.9995 can be represented in the system with a resolution of 0.0005. The system runs with a clock of 1000 Hz, which is the same frequency as sampling in the dataset.

The output of the system has five flags: (1) spike detector threshold calculated, (2) spike detected, (3) event detected, (4) HVSW classification, and (5) HPD classification. The threshold flag indicates if a threshold for the spike detector has been calculated. The

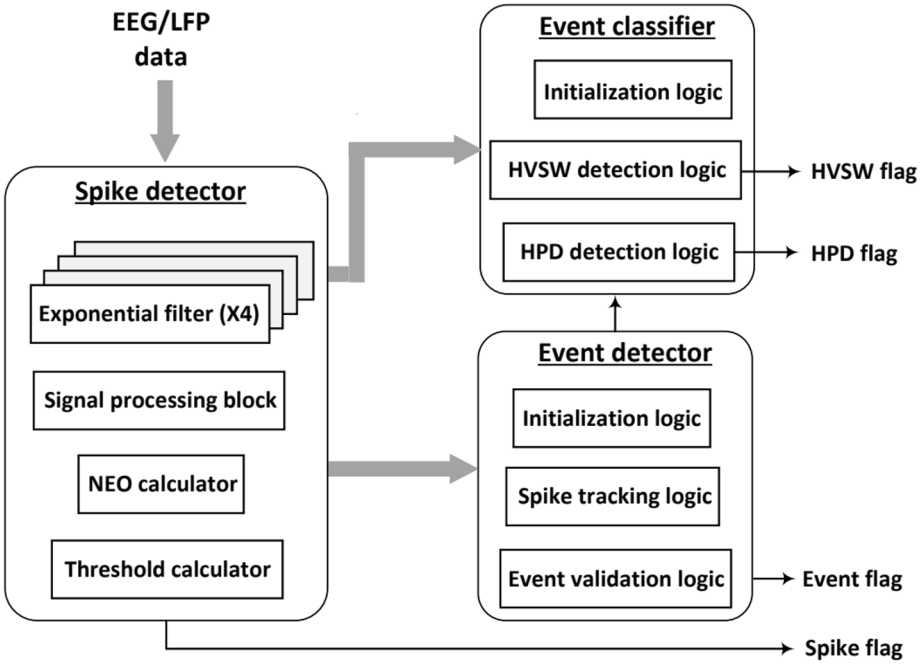

Fig. 5 Block diagram of the epileptiform activity detector and classifier implemented in hardware

flags for event detection, HPD and HVSW classification have a delay of 5 s. This is due to the requirement for an event to have a duration of at least 5 s.

4.1 Spike detector

The spike detector is based on the block diagram highlighted in Fig. 3 and is adjusted to suit hardware-efficient implementation. This section will go over the IIR filter and the σ_n estimator implementations as those vary from what was explained in Sect. 3.1.2.

4.1.1 Infinite impulse response filters

The IIR filters, described by Equation 2, can be implemented more efficiently when using binary values. As $\alpha < 1$, a multiplication is performed by the numerator and a division is performed by the denominator. This division can be replaced by binary right shifts which is shown in Equation 6, where $G1$ and $G2$ are the nominators and $1/(2^S)$ denotes a right bit shift by S. Table 4 shows the implemented filters and their respective gains and shift values.

$$y(n) = G_1 \frac{x(n-1)}{2^S} + G_2 \frac{y(n-1)}{2^S} \tag{6}$$

4.1.2 σ_n estimator

Calculating the MAD as shown in Equation 4 is a costly operation as taking the median over a window needs a lot of memory allocation. Yang and Mason [26] introduced a hardware-efficient implementation for estimating σ_n by following the statistical theory that the probability of Gaussian noise exceeding σ_n is known to be 0.159. Figure 6 shows the block diagram of the σ_n estimator. The input signal is compared with the estimated σ_n, σ_n^{est}, and outputs a $'1'$ if the input signal is greater. The amount of $'1's$ inside a window of size M is counted and subtracted from $0.159 \times M$. This result is fed into a digital integrator and is then used to update σ_n^{est} every M clock cycles. The loop keeps updating until a convergence is detected after which the converged value σ_n is output by the system.

4.2 Epileptiform event detector

In Sect. 3.2 the proposed epileptiform event detector is described, which is visualized by the flowchart in Fig. 4, where the green and purple elements are implemented in the hardware. The yellow elements of the detector were left out of the hardware implementation as the implementation should be real-time and efficient. Changes made to the working of the event detector are highlighted in this section.

4.2.1 Amplitude calculation and check

The amplitude calculation and check have been left out of the hardware implementation to support a real-time system and to save area on memory. The amplitude calculation is required for both the negative and positive peaks and requires two comparisons per

Table 4 The values for the IIR filters implemented in hardware using two gains and a binary shift

	Value of G1	Value of G2	Value of S
Filter 1	2	510	9
Filter 2	3	1	2
Filter 3	3	29	5

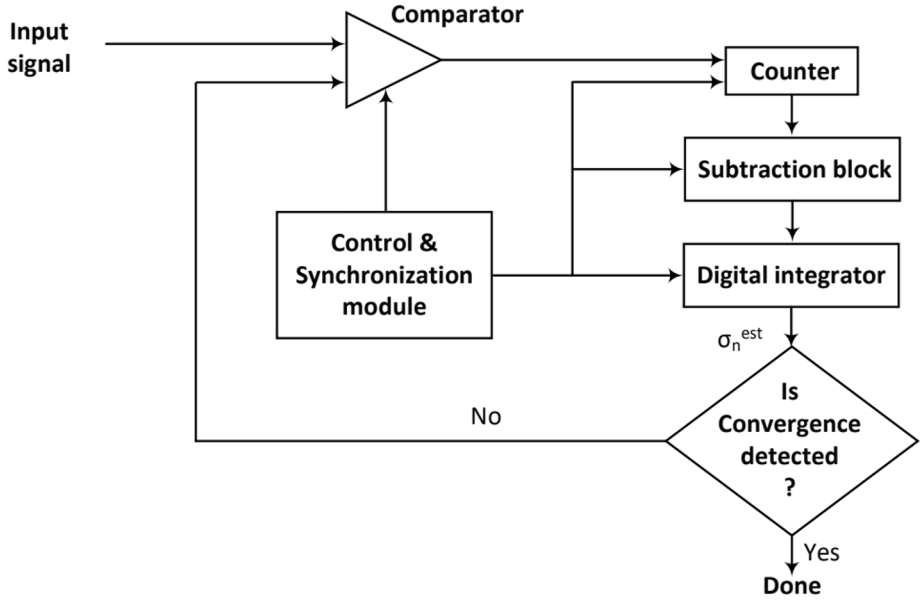

Fig. 6 Block diagram of the estimation of σ_n implemented in hardware

sample for the 100 samples after a spike is detected. The baseline amplitude calculation requires the calculation of the 97th percentile of 20, 000 continuous samples. Both these calculations require significant area for memory and the baseline amplitude calculation can negatively affect the future near real-time behavior of the system. The negative impact on the (near) real-time behavior is caused by the fact that a segment of 20 s without any spikes needs to be found before the calculation can be performed, resulting in an idle time before events can be detected.

4.2.2 Nested loop

The nested detection loop, shown in Fig. 4, is indicated by the yellow element containing $spike = \text{“}1^{st}\ spike'' + 1$. This implementation mostly impacts the (near) real-time working of the system but also requires extra memory. The real-time working of the system is impacted greatly by the nested loop as it starts event detection using a previous spike. This helps with the correct detection of the start and end of events but will cause extra delay if added, which is undesirable for a near real-time system.

4.2.3 Preliminary spikes check

The preliminary spikes check was introduced, as explained in Sect. 3.2.3, to correctly detect the start of HPD events. Hardware implementation of this function is not viable as the algorithmic, non-real-time implementation, checks the spikes in front of a detected event to correct the detection. If this were to be implemented in the hardware, a delay of the longest detectable event needs to be added to show a detected event with preliminary spikes, which would result in the system not running real-time. The effect of leaving out the preliminary spikes check is that the beginning of some HPD events will not be detected correctly.

4.3 Epileptiform event classifier

The epileptiform event classifier is also simplified with respect to the presented version in Sect. 3.3; that is, the events are classified into only HVSW and HPD events as these are the most important elements relevant for the development of epilepsy. As explained in Sect. 3.3, an event will be classified automatically as an HVSW event unless 5 continuous seconds with at least 25 spikes are detected. The classifier is implemented using a ring buffer, which saves the moment in time when a spike is detected. Using the ring buffer the number of spikes in the previous 5 s is tracked, when the event detection flag goes high a check on the amount of spikes determines the classification. During the time the event detection flag is high, the classification can change from HVSW to HPD if the number of spikes in the buffer reaches 25. The classification relies on event detection and thus has a delay of at least 5 s, the maximum delay is not known as this can be the length of an entire epileptiform event if the last 5 s contain 25 spikes.

To address the variability and noise inherent in the LFP signal, particularly across electrodes and subjects, our methodology parametrizes key criteria such as spike duration and frequency, enabling flexible tuning based on experimental context. This approach improves robustness and adaptability, reducing the risk of misclassifying borderline events. Furthermore, the parameterized structure can support future integration of adaptive thresholding mechanisms, as demonstrated in our previous work using an adaptive multi-threshold encoding for spiking neural network application [4]. This design choice lays the groundwork for developing a more automated and generalizable system for future near real-time epileptiform activity detection and classification.

5 Experimental setup

5.1 Performance metrics

The performance results of the spike detector, event detector, and event classifier are represented using one or more of the following metrics. (1) Accuracy, which indicates the rate of correct detections or classifications, illustrated in Equation 7 and given in percentage. (2) Sensitivity, as part of Equation 8, showing the rate of positive detections or classifications, which are correctly identified. (3) Precision, as part of Equation 9, indicating the number of true detections or classifications over the total number of true events. These metrics make use of True Positive (TP), False Positive (FP), and False Negative (FN) detection. True Negative (TN) is not considered as this results in a large bias. The formulas for the three metrics are shown below.

$$Accuracy = \frac{TP}{TP + FP + FN} \tag{7}$$

$$Sensitivity = \frac{TP}{TP + FN} \tag{8}$$

$$Precision = \frac{TP}{TP + FP} \tag{9}$$

5.2 Spike detector

The spike detector is evaluated using a synthetic dataset which consists of 8 recordings of 48 h with noise levels ranging from 0.05 dB to 0.2 dB at an interval of 0.05 dB [18]. The naming structure used for the different datasets starts with E (easy) or D (difficult),

which refers to the difficulty level of clustering the spikes (not important for this work) and ends with the value of the noise level. With these datasets, the proposed spike detector can be evaluated and compared to three different methods: the standard implementation of NEO and ANT, ASO [28], and DWT [16]. As the implementations of ASO and DWT only have results on accuracy this is the only metric used to evaluate performance.

5.3 Event detector and classifier

The output of the epileptiform event detector and classifier were reviewed by an animal epilepsy expert (G.K.), who indicated the TP, FP and FN detections and classifications from which the performance metrics were calculated. For the event detector 48 h and for the classifier 108 h of input EEG/LFP recordings from the IHKA model were used, originating from 8 and 9 mice, respectively. After the evaluation of the event detector, the algorithm has been adjusted, and with the new version the event classifier has been evaluated.

5.4 Hardware implementation

The development flow of the hardware implementation is shown in Fig. 7. The algorithm was first developed in Python and has been implemented in the hardware description languages (HDL) of Verilog and very high speed integrated circuit (VHSIC) program hardware description language (VHDL). The python algorithm was manually verified after which the hardware simulations done in Questasim were compared to verify correct working. The process is split up into the workflow of the development of an ASIC and of an FPGA.

5.4.1 Application specific integrated circuit

Using Cadence Genus, a worst corner synthesis of the design was done with the TSMC 40 nm library. The system clock frequency was set to a frequency of 5000 Hz, which is

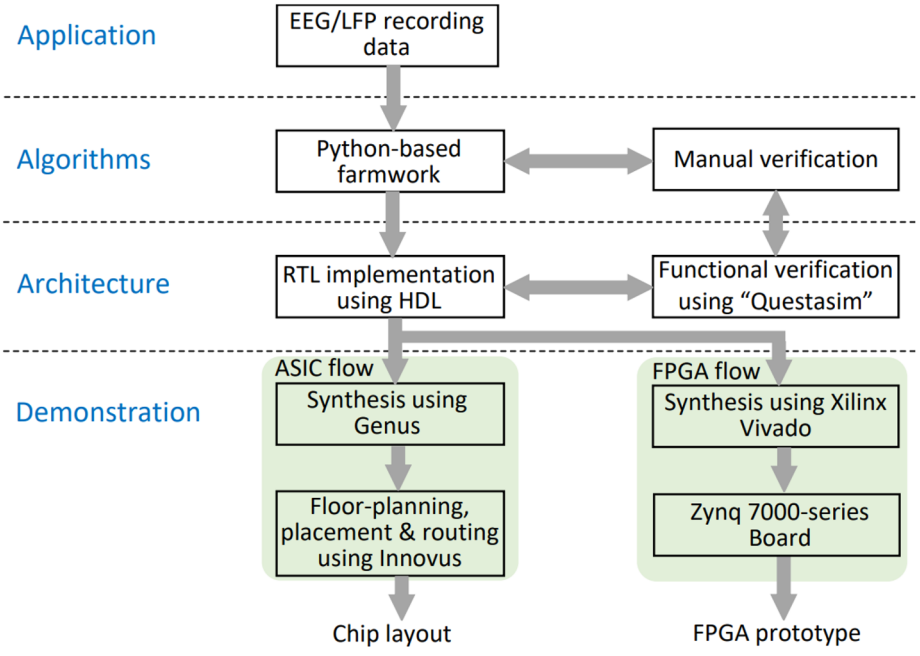

Fig. 7 Development flow of the hardware implementation

the lowest clock frequency allowed by Genus. From the worst corner analysis, results on area and power were generated for the spike detector, event detector, event classifier, and the full design. Using the synthesized design a place and route was made using Cadence Innovus using a density of 0.7 and the post-layout results in realistic results on power and area.

5.4.2 Field programmable gate array

The design has been synthesized using Xilinx Vivado for a demonstration on a PYNQ-Z1 board containing a ZYNQ-7000 series FPGA. The clock of the system is set to 1000 Hz and 300,000 16-bit values in two s complement and fixed point representation are loaded into the BRAM and used as input signal. The synthesis for the FPGA gives results on power usage and area, which is reported in the available logic blocks on the FPGA.

6 Results

6.1 Spike detector

The results of the four spike detection methods (see Table 2) were compared with box plots in Fig. 8. The Wavelet transform (DWT) was found to have an average accuracy of 89.5%, whereas ASO had an average accuracy of 91.1%. Both the standard and improved version of the NEO and ANT implementation achieved a higher accuracy, the standard version had an accuracy of 92.9%, while the improved version had an accuracy of 93.3%. This is a marginal improvement achieved by removal of the temporal drift. The improvement was achieved using an IIR filter that was originally implemented to allow spike amplitude calculations, and because of this, no overhead is added to the spike detection. Next to the fact that the improved version achieved the highest accuracy, it is also clear that the minimum and maximum accuracy values are closer to each other, indicating this method is more stable. This suggests that this method is indeed robust to noise, which was one of the requirements for the spike detector.

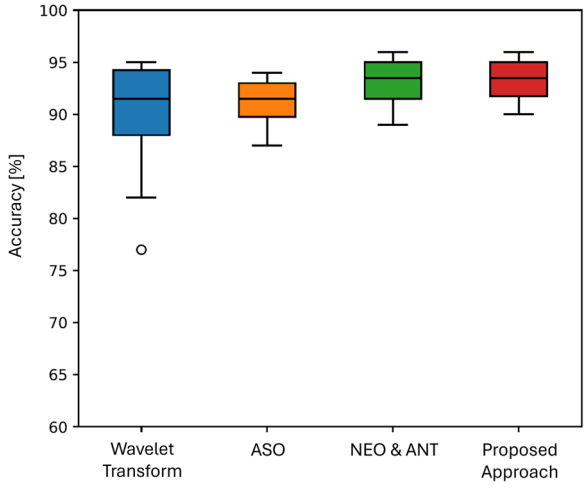

Fig. 8 Accuracy of spike detection of the proposed approach (in red, right) with three existing spike detection methods, i.e., wavelet transform (DWT), ASO and combined NEO & ANT (see also qualitative features of these and other existing methods in Table 2)

6.2 Epileptiform event detector

We next conducted a detailed quantitative analysis to benchmark of our automated event detection and classification approach, using standard performance metrics such as accuracy, sensitivity, and precision. Figure 9 shows the accuracy, sensitivity and precision retrieved from the manual analysis of the output of 48 h of input data to the epileptiform event detector. The event detector had an average accuracy of 93.6%, with a precision of 99.0% and a sensitivity of 94.0%. From Fig. 9 it is clear that there is one outlier for both accuracy and sensitivity results, corresponding to the same dataset. The low sensitivity indicates that a lot of events were missed in detection. During the manual analysis of this dataset, it became clear that the spike detection accuracy for this dataset was not high enough to support accurate event detection. As the event detection fully relies on the spike detection an improvement was made to the spike detector. The improvement entails the ability to adjust the scalar C from Equation 3. This results in some manual work during analysis, but the option to adapt spike detector provides flexibility to achieve better overall results on sensitivity and accuracy.

6.3 Epileptiform event classifier

The results from the manual analysis of 108 h of EEG recording (input data) for the event classifier are shown on the right in Fig. 9. For the manual analysis, identification of epileptiform events was based on the criteria described by [23], and performed manually with substantial agreement (Cohen s kappa 0.81) based on independent analysis of half of the data-set (i.e. 54 h) by two raters. In the analysis of the event classifier, the ability to adjust the scalar C in the spike detector was included. The event classifier had an accuracy of 95.8% with a sensitivity of 95.8% and a precision of 95.8%. When comparing the results on detection and classification in Fig. 9, we can see that the classifier achieves a higher consistency over the three metrics on all the datasets. The consistency is visible in the small spread indicated by the quartile and maximum data values for classification. The results are directly correlated as both the detector and classifier fully rely on the spike detector. However, we cannot directly compare both results and give an impact value to the added ability to adjust scalar C. Still, this stability in the classifier results

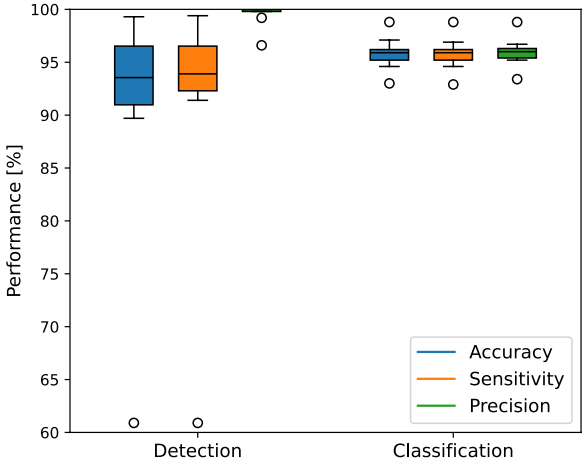

Fig. 9 Illustration of accuracy, sensitivity and precision results from both the epileptiform event detector (on the left) and classifier (on the right) extracted using the automated algorithm compared to the manual analysis of the same 48 h of ipsilateral hippocampal LFP data

Table 5 Manual analysis time versus computational time for LFP recordings

Time to get input data	108 h
Time for manual analysis	27 h
Computation time	20 min
Time reduction	98.8%

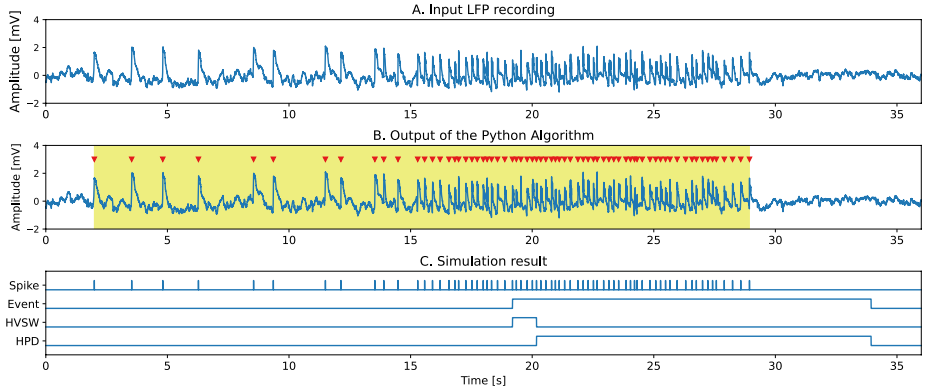

Fig. 10 Output results of both the algorithm, and its hardware implementation. **a** Input LFP recording. **b** The output of the algorithmic implementation in Python: red markers indicate the detected spikes, the coloured area indicates the detected event, and the colour indicates the classification. **c** Output signals of the hardware simulation where *Spike* indicates a detected spike, *Event* a detected event and *HVSW* and *HPD* represent the classification of a detected event

shows that the adjustment of scalar C positively impacts the results with little manual work added.

6.4 Complete system for automated epileptiform activity detection

The automated epileptiform activity detector and classifier reduced analysis time of the 108 h of LFP data to just 20 min, compared to 27 h required for manual analysis, resulting in a 98.8% time saving, as described in Table 5. Secondly, the epileptiform activity detector and classifier achieved a constant high level of detection and classification accuracy, which removed the dependability on expert analysis and removed inter-observer biases and errors. Our approach achieved a superior sensitivity of 94.0% for detection and 95.8% for classification over the approach introduced by [22] that achieved a sensitivity of 86–90%. The achieved time reduction of >80% by [22] was also lower than the 98.8% in the current work, which can be explained by the almost fully automated implementation of our work.

6.5 Application specific integrated circuit

A demonstration of future real-time event detection is shown in Fig. 10 showing the output signals of the hardware simulation as detected spikes and classified events. The response time of the detection and classification is demonstrated through the hardware simulation outputs, where spikes, events, and their respective classifications where HVSW and HPD are near-instantly (i.e. for 1 min of data producing output within 0.2 s) generated, highlighting the system's capability for near real-time signal analysis. The area and power consumption results gathered from the synthesis are shown in Fig. 11, which shows that the spike detector together with the interconnect takes up the biggest part of the area and uses the most power. Moreover, it is clear that the distribution in area

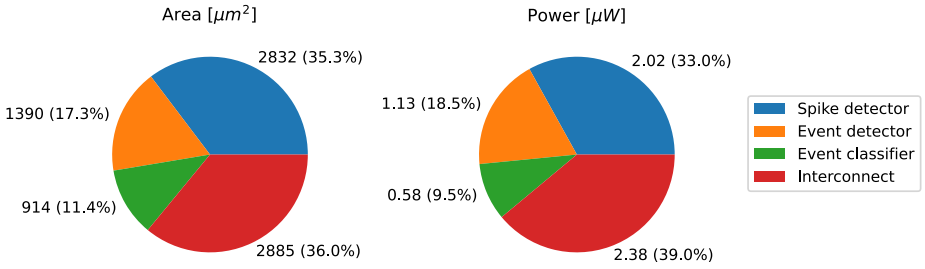

Fig. 11 Area and power consumption results from the synthesis of the design using Genus and TSMC 40nm library

Table 6 Chip area and power consumption results of the placed and routed design and the FPGA implementation

	ASIC	**FPGA**
Tool	Cadence Genus	Xilinx Vivado
Technology	TSMC 45 nm	PYNQ-Z1 board with ZYNQ-7000 FPGA
Supply voltage	1.0 V	1.00 V
Clock	5000 Hz	1000 Hz
Area	9114 μm^2	815 LUTs 427 Registers 8 DSPs
Static power	6.66 µW	114 *mW*
Dynamic power	16.09 µW	58 *mW*

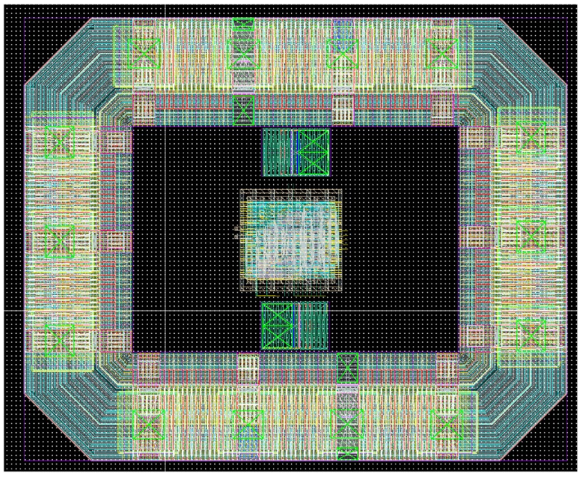

Fig. 12 Layout of the physical design

and power usage are correlated, as the percentage per part of the design is almost equal. The area of the spike detector could be reduced by decreasing the input bit size, which resulted in a lower resolution throughout the system, as everywhere the size of the input signal Is used.

The area and power results of the place and route are shown in Table 6 from which it is evident that the ASIC design reached an area of 9114 μm^2 that is 13.6% larger than the synthesis achieved. This is because an ASIC gives a more realistic result on area, as the netlist resulting from the synthesis is realistically routed in the design. The layout gathered from the place and route is shown in Fig. 12. External memory blocks (e.g., SRAM and DRAM) are not integrated, as inputs were directly applied to the system for

this proof-of-concept, and thus no performance metrics provided on these aspects. This choice simplifies the architecture but limits the completeness of performance metrics at full system-level.

6.6 Field programmable gate array

The algorithm was successfully implemented on an FPGA to show the working as a Brain Machine Interface (BMI). All the outputs of the system are routed to LEDs, the input data is stored on the BRAM, and the reset is linked to a switch. The area and power results are reported in Table 6 in addition to the ASIC results; although a direct comparison is not possible as both implementations make use of different technologies, a realistic image is given if one of two implementations is further developed.

7 Conclusion

In this paper, we propose a new method for the detection and classification of epileptiform activity using data from EEG/LFP recordings gathered from a preclinical study, in this case of the IHKA mouse model. Our method is based on a spike detection stage, which is followed by an epileptiform event detector that uses a general description of all types of epileptiform events. The last stage is an epileptiform event classifier, which classifies events based on their duration and intra-event spike frequency into one of four groups. The detection and classification algorithm is implemented in Python and was found to reach a general epileptiform event detection accuracy of 93.1%. Epileptiform events were classified with an accuracy of 95.8%, and the implemented algorithm yielded a time reduction of 98.8% compared to manual analysis. Our approach achieved equal or better accuracy over existing epileptiform event detection methods described in the literature, but most of all, yielded a superior time reduction that was possible as the algorithm is automated to a level exceeding that of existing methods due to a minimal manual input. Real-time hardware implementation of the algorithm was developed using HDL. Power and area results were gathered using the TSMC 40nm library and a Zynq 7000-series FPGA. The work was demonstrated using the FPGA, which shows the potential of a brain-machine interface (BMI). Overall, our detection approach has the potential to streamline research and accelerate advancements in epilepsy studies by providing a complete package that includes a spike detector, epileptiform event detector and classifier with better accuracy while significant reduction in the analysis time. Because our epileptiform event detection algorithm can be tailored to different spike and event criteria, it holds promise for broader use in additional preclinical epilepsy models as well as future clinical applications with scalp EEG data.

Author contributions

J.V. developed the algorithm and hardware solutions for this work, G.K. performed the clinical experiments and both wrote the main manuscript, both J.V. and G.K. contributed equally to this work. S.D. gave guidance at hardware level and supported for Figure 12. R.B. was leading this work and did text and figure editing. M.A.S., A.M.J.M.v.d.M., S.H. and E.A.T. has provided their comments. All authors also reviewed the manuscript.

Funding

This work was supported by the Dutch National Epilepsy Foundation (WAR 22-07) to A.M.J.M.v.d.M. and E.A.T.), the European Union Joint Programme - Neurodegenerative Disease Research project REBALANCE (no 10510062210003 to E.A.T and A.M.J.M.v.d.M.), the Medical Delta program "Medical NeuroDelta: Ambulant Neuromonitoring for Prevention and Treatment of Brain Disease" (to A.M.J.M.v.d.M.) and financial support from Corcept Therapeutics (to E.A.T and A.M.J.M.v.d.M.). This work is also partially funded by the European Union, DAIS (Grant No. 101007273), NEUROKIT2E (Grant No. 101112268), and supported by the TU Delft AI labs program.

Data availability

Data are available from senior authors Rajendra Bishnoi and Else Tolner, upon reasonable request.

Declarations

Ethics approval and consent to participate
All animal experimental procedures were approved by the local and national animal ethical committees (i.e., the LUMC Animal Welfare Body and the Dutch Central Authority for Scientific Procedures on Animals CCD (project license AVD11600202317073) following recommendations of the European Communities Council Directive (2010/63/EU) and performed in accordance with ARRIVE guidelines.

Consent to publish
All authors have reviewed and approved the final version of the manuscript and have given their consent for the article to be published.

Consent to participate
Not applicable.

Clinical trial details
Not applicable.

Competing interest
The authors declare no competing interest.

Received: 13 March 2025 / Accepted: 23 July 2025
Published online: 26 September 2025

References

1. Anjum SMM, Käufer C, Hopfengärtner R, Waltl I, Bröer S, Löscher W. Automated quantification of EEG spikes and spike clusters as a new read out in Theiler's virus mouse model of encephalitis-induced epilepsy. Epilepsy Behav. 2018;88:189–204.
2. Bergstrom RA, Choi JH, Manduca A, Shin H-S, Worrell GA, Howe CL. Automated identification of multiple seizure-related and interictal epileptiform event types in the EEG of mice. Sci Rep. 2013;3(1):1483.
3. Bouilleret V, Ridoux V, Depaulis A, Marescaux C, Nehlig A, Salle G. Recurrent seizures and hippocampal sclerosis following intrahippocampal Kainate injection in adult mice: electroencephalography, histopathology and synaptic reorganization similar to mesial temporal lobe epilepsy. Neuroscience. 1999;89(3):717–29. https://doi.org/10.1016/S0306-4522(98)00401-1.
4. Diware S, Dong Y, Yaldagard M, Hamdioui S, Bishnoi R. Adaptive multi-threshold encoding for energy-efficient ecg classification architecture using spiking neural network. Design, automation and test in Europe (DATE); 2025.
5. Duveau V, Pouyatos B, Bressand K, Bouyssières C, Chabrol T, Roche Y, Depaulis A, Roucard C. Differential effects of antiepileptic drugs on focal seizures in the intrahippocampal Kainate mouse model of mesial temporal lobe epilepsy. CNS Neurosci Therap. 2016;22(6):497–506.
6. Harrison R. A low-power integrated circuit for adaptive detection of action potentials in noisy signals. In: Proceedings of the 25th annual international conference of the IEEE engineering in medicine and biology society (IEEE Cat. No.03CH37439), vol 4, pp. 3325–3328. 2003. https://doi.org/10.1109/IEMBS.2003.1280856.
7. Kwan P, Brodie MJ. Early identification of refractory epilepsy. N Engl J Med. 2000;342(5):314–9.
8. Kyle JJ, Sharma S, Tiarks G, Rodriguez S, Bassuk AG. Fast detection and quantification of interictal spikes and seizures in a rodent model of epilepsy using an automated algorithm. Bio-Protoc. 2023;13(6): e4632.
9. Laxer KD, Trinka E, Hirsch LJ, Cendes F, Langfitt J, Delanty N, Resnick T, Benbadis SR. The consequences of refractory epilepsy and its treatment. Epilepsy Behav. 2014;37:59–70.
10. Lévesque M, Avoli M. The kainic acid model of temporal lobe epilepsy. Neurosci Biobehav Rev. 2013;37(10):2887–99.
11. Lisgaras CP, Scharfman HE. Robust chronic convulsive seizures, high frequency oscillations, and human seizure onset patterns in an intrahippocampal kainic acid model in mice. Neurobiol Dis. 2022;166: 105637.
12. Milligan TA. Epilepsy: a clinical overview. Am J Med. 2021;134(7):840–7.
13. Mukhopadhyay S, Ray G. A new interpretation of nonlinear energy operator and its efficacy in spike detection. IEEE Trans Biomed Eng. 1998;45(2):180–7. https://doi.org/10.1109/10.661266.
14. NeuroScore. 2024. https://www.datasci.com/products/software/neuroscore.
15. NeuroWorks. 2024. https://natus.com/neuro/eeg-aeeg/eeg-software/.
16. Ocak H. Automatic detection of epileptic seizures in EEG using discrete wavelet transform and approximate entropy. Expert Syst Appl. 2009;36(2):2027–36. https://doi.org/10.1016/j.eswa.2007.12.065.
17. Prasanth T, Thomas J, Yuvaraj R, Jing J, Cash SS, Chaudhari R, Leng TY, Rathakrishnan R, Rohit S, Saini V, Westover BM, Dauwels J. Deep learning for interictal epileptiform spike detection from scalp EEG frequency sub bands. In: 2020 42nd Annual international conference of the ieee engineering in medicine and biology society (EMBC), 2020. pp. 3703–3706. https://doi.org/10.1109/EMBC44109.2020.9175644.
18. Quiroga RQ, Nadasdy Z, Ben-Shaul Y. Unsupervised spike detection and sorting with wavelets and superparamagnetic clustering. Neural Comput. 2004;16(8):1661–87.
19. Racine RJ. Modification of seizure activity by electrical stimulation motor: II. Seizure. Electroencephalogr Clin Neurophysiol. 1972;32(3):281–94.
20. Rizk M, Wolf PD. Optimizing the automatic selection of spike detection thresholds using a multiple of the noise level. Med Biol Eng Comput. 2009;47:955–66.
21. Stafstrom CE, Carmant L. Seizures and epilepsy: an overview for neuroscientists. Cold Spring Harb Perspect Med. 2015;5(6): a022426.
22. Theilmann W, Gericke B, Schidlitzki A, Anjum SMM, Borsdorf S, Harries T, Roberds SL, Aguiar DJ, Brunner D, Leiser SC, et al. Novel brain permeant mtorc1/2 inhibitors are as efficacious as rapamycin or everolimus in mouse models of acquired partial epilepsy and tuberous sclerosis complex. Neuropharmacology. 2020;180: 108297.

23. Twele F, Töllner K, Bankstahl M, Löscher W. The effects of carbamazepine in the intrahippocampal Kainate model of temporal lobe epilepsy depend on seizure definition and mouse strain. Epilepsia Open. 2016;1(1–2):45–60.
24. Wei L, Boutouil H, Gerbatin RR, Mamad O, Heiland M, Reschke CR, Del Gallo F, Fabene PF, Henshall DC, Lowery M, et al. Detection of spontaneous seizures in EEGS in multiple experimental mouse models of epilepsy. J Neural Eng. 2021;18(5): 056060.
25. Welzel L, Schidlitzki A, Twele F, Anjum M, Löscher W. A face-to-face comparison of the intra-amygdala and intrahippocampal Kainate mouse models of mesial temporal lobe epilepsy and their utility for testing novel therapies. Epilepsia. 2020;61(1):157–70.
26. Yang Y, Mason AJ. Hardware efficient automatic thresholding for neo-based neural spike detection. IEEE Trans Biomed Eng. 2017;64(4):826–33. https://doi.org/10.1109/TBME.2016.2580319.
27. Zeidler Z, Brandt-Fontaine M, Leintz C, Krook-Magnuson C, Netoff T, Krook-Magnuson E. Targeting the mouse ventral hippocampus in the intrahippocampal kainic acid model of temporal lobe epilepsy. Eneuro. 2018;5(4):32.
28. Zhang Z, Constandinou TG. Adaptive spike detection and hardware optimization towards autonomous, high-channel-count BMIS. J Neurosci Methods. 2021;354: 109103.

Publisher's Note